We are IntechOpen, the world's leading publisher of Open Access books Built by scientists, for scientists

4,800
Open access books available

122,000
International authors and editors

135M
Downloads

Our authors are among the

154
Countries delivered to

TOP 1%
most cited scientists

12.2%
Contributors from top 500 universities

CLARIVATE ANALYTICS BOOK CITATION INDEX INDEXED

WEB OF SCIENCE™

Selection of our books indexed in the Book Citation Index in Web of Science™ Core Collection (BKCI)

Interested in publishing with us?
Contact book.department@intechopen.com

Numbers displayed above are based on latest data collected.
For more information visit www.intechopen.com

2

Enhanced Diffuse Reflection of Light by Using a Periodically Textured Stainless Steel Substrate

Shuo-Jen Lee and Wen-Cheng Ke
Yuan Ze University, Taiwan, R.O.C.

1. Introduction

The flexible solar cells fabricated on a stainless steel substrate are being widely used for the building of integrated photovoltaics (BIPVs) in recent years. Because stainless steel has many advantages, such as low cost, high extension, ease of preparing etc. It was believed that the wide application of BIPVs especially rooftop applications, would be the biggest market for flexible PV technology (Kang et al. 2006, Otte et al. 2006, Chau et al. 2010, Fung et al. 2008). Until now, one of the main challenges of the BIPVs remains how to improve the conversion efficiency. Since, the path length of the photovoltaic effect is considerable shorter in a thin film solar cell resulting in reduced efficiency. Many researchers have focused on light trapping, and have adopted a different TCO technology, such as LP-CVD, PVD, to increase the path length of the incoming light, and improve the photovoltaic conversion efficiency of thin film solar cells (Selvan et al. 2006, Llopis et al. 2005, Söderström et al. 2008, Müller et al. 2004). Moreover, light trapping provides some significant advantages including, reduction of the cell thickness, reduced processing time and reduced cost, improved cell efficiency and the improved stability of amorphous Si (a-Si:H).

The idea of trapping light inside a semiconductor by total internal reflection was reported by John in 1965 (John 1965). It also indicated that the effective absorption of a textured semiconductor film could be enhanced by as much as a factor of 60 over a plane-parallel film (Yablonovitch and Cody 1982). It should be mentioned that a major limitation to thin film solar cell efficiency is the long absorption length of the long wavelength photons and the low thickness of the absorber layer. The absorption length of amorphous silicon (a-Si:H) with a bandgap of 1.6 eV, for red and infrared solar photons, exceeds 1 μm and 100 μm, respectively (Ferlanto et al. 2002, Zhou and Biswas 2008). However, for a-Si:H the hole diffusion length is ~300-400 nm, which limits the solar cell absorber layer thickness to less than the hole diffusion length (Curtin et al., 2009). This makes it exceedingly difficult to harvest these photons since the absorber thickness of a p-i-n single junction solar cell is limited to only a few hundred nanometers for efficient carrier collection. In addition, the low-cost approach of thin-film silicon solar cells is very sensitive to film thickness, since the throughput increases with the decrease in layer thickness. Thus, sophisticated light trapping is an essential requirement for the design of thin-film solar cells (Rech et al., 2002).

Enhanced light-trapping in thin film solar cells is typically achieved by a textured metal backreflector that scatters light within the absorbing layer and increases the optical path length of the solar photons. In our recent researches [Lee et al., 2009], various processing

techniques including, electro-polishing, sandblasting, photolithography, lift-off and wet-chemical etching were used to create periodically textured structures on the different types of stainless steel substrates. The relationships between the surface morphology of textured stainless steel substrate and optical properties will be carefully discussed.

2. Surface treatment of texturing stainless steel substrate

2.1 Electro-polishing process

In this study, electrochemical processing was used to achieve sub-micro texturing stainless steel substrate base on the fundamental electrochemical reaction items as (1)-(3).
Anode chemical reaction:

$$Fe^{2+}+2(OH)^{-}\rightarrow Fe(OH)_2 \text{ or } Fe(OH)_3 \quad (1)$$

$$OH^{-}\rightarrow O_2\uparrow+H_2 \text{ (Parasitic reaction)} \quad (2)$$

Cathode chemical reaction:

$$2H^{+}\rightarrow H_2\uparrow \quad (3)$$

The electro-polishing system is shown in Fig. 1. The important parameters are as follows:

1. Substrate clean by acid-washing in H_2O_2:H_2SO_4=1:3 solution.
2. Electrolyte solution (Na_2SO_4) with concentration of 60-100 (g/L).
3. Current density in electro-polishing (EP) process is 0.1-1.0 (A/cm^2).

The clamp was used to hold the anode and cathode plates. The anode and cathode plates were separated by Teflon with thickness of 1 cm. Fig. 2 shows the optical microscopy (OM) images of 304 SS substrate with and without EP process. The average surface roughness (Ra) of 304 SS substrate increased from 0.045 μm to 0.197 μm after the EP process with current density of 1A/cm^2 in 10 min.

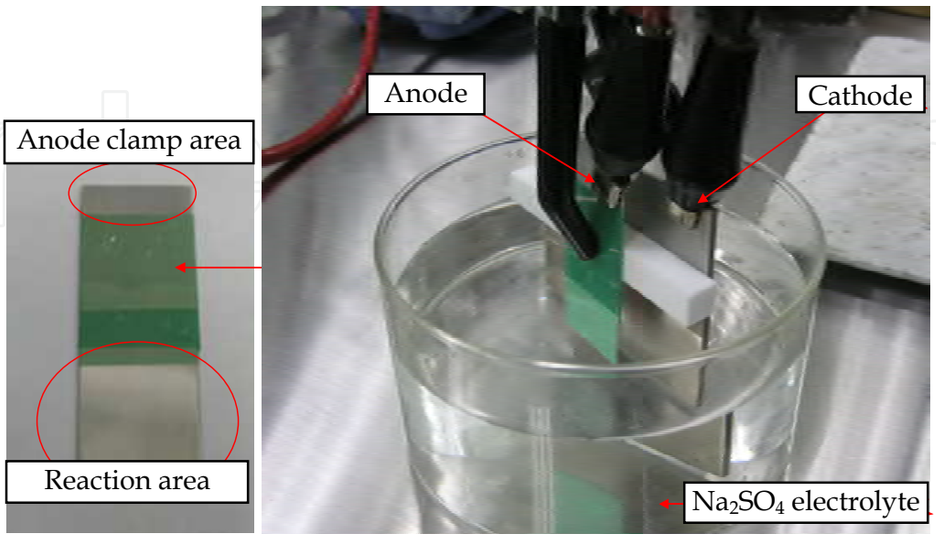

Fig. 1. Experimental set-up of the EP process.

2.2 Sand blasting process

The glass sand (#320) was used to form randomly textured surface with cave size of several μm to tens μm on the surface of stainless steel substrate. The average surface roughness (Ra) of 304 SS substrate increased from 0.277 μm to 6.535 μm after the sand blasting process. The OM images of raw 304 SS substrate and with sand blasting process were shown in Fig. 3.

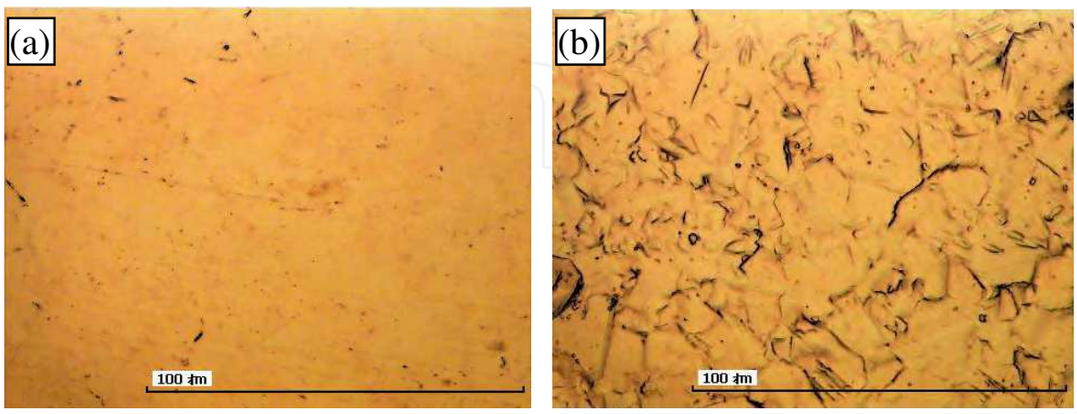

Fig. 2. The OM images (x2000) of (a) raw 304 SS substrate surface and (b) 304 SS substrate surface with EP process.

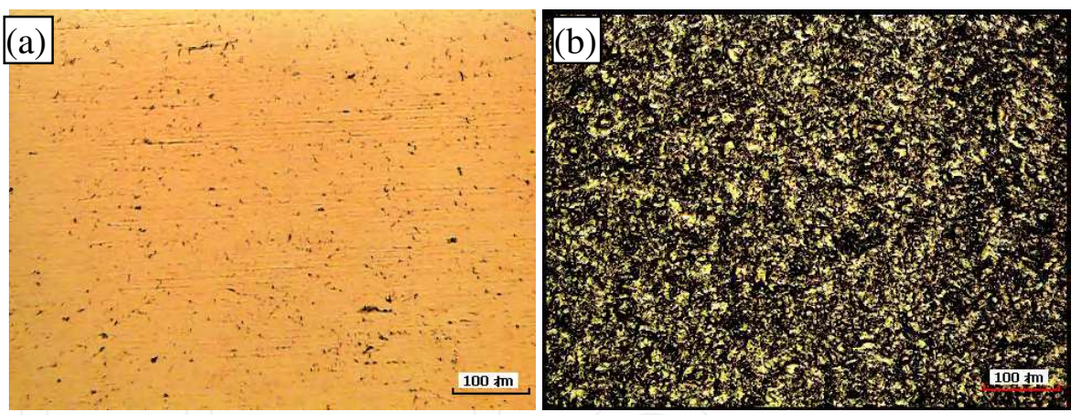

Fig. 3. The OM images (x400) of (a) raw 304 SS substrate surface and (b) 304 SS substrate surface with sand blasting process.

2.3 Photolithography process

The photo-mask patterns were designed by CAD. Photolithography is a process of using light to transfer a geometric pattern from a photo-mask to a photo-resist on a 430BA SS substrate. The steps involved in the photolithographic process are metal cleaning, barrier layer formation, photo-resist application, soft baking, mask alignment, exposure and development, and hard-baking. After the photolithographic process, the 430BA SS substrate is etched by aqua regia (HNO_3 : HCl=1 : 3). There are two types of photo-mask patterns: one, different diameters but with the same interval, and two, the same diameters but with a different interval. They are both designed to study light trapping for the application of thin film solar cells. Finally, silver coating technique by e-beam evaporation was used to improve the TR and DR rates of the 430BA SS substrate.

2.4 Lift-off and etching process

In this study, lift-off and etching processes were used to fabricate the different textures of the 304BA SS substrates. The striped texture was created on the 304BA SS substrate using the lift-off process. After the hard-baking process, a silver (Ag) thin film was deposited on the substrate by e-beam evaporation. An acetone solution was used to remove the residual photo resistor (PR). The depth of the striped texture was controlled by the thickness of the Ag thin film deposited. Four different striped textures were created on the 304BA SS substrates, including period/height: 6/0.1, 6/0.3, 12/0.1 and 12/0.3 μm. Two other types of textured 304BA SS substrate, the ridged-stripe and pyramid texture with 22.5 μm width were created by the etching process. After hard-baking, the 304BA SS substrate was etched by aqua regia (HNO_3 : HCl : DI water＝1 : 3 : 4). The etching temperature was 28-35℃ with an etching time of 7-12 min. to control the etching depth of the textured 304BA SS substrate. The detail experimental flow charts of lift-off and etching processes are shown in Fig. 4 and Fig. 5, respectively.

3. Optical properties of textured stainless steel substrate

3.1 Measurements of optical properties of textured stainless steel substrate

The total reflection (TR) and diffuse reflection (DR) rates of incident light from the textured substrate were carefully studied by using a Perkin Elmer Lambda 750S spectrometer. It was known that the specula reflection takes place on a smooth surface, and the angle of reflection is the same as the angle of incidence. DR is a phenomenon where an incident beam of light strikes an uneven or granular surface and then scatters in all directions. In Fig. 6, the 6 cm

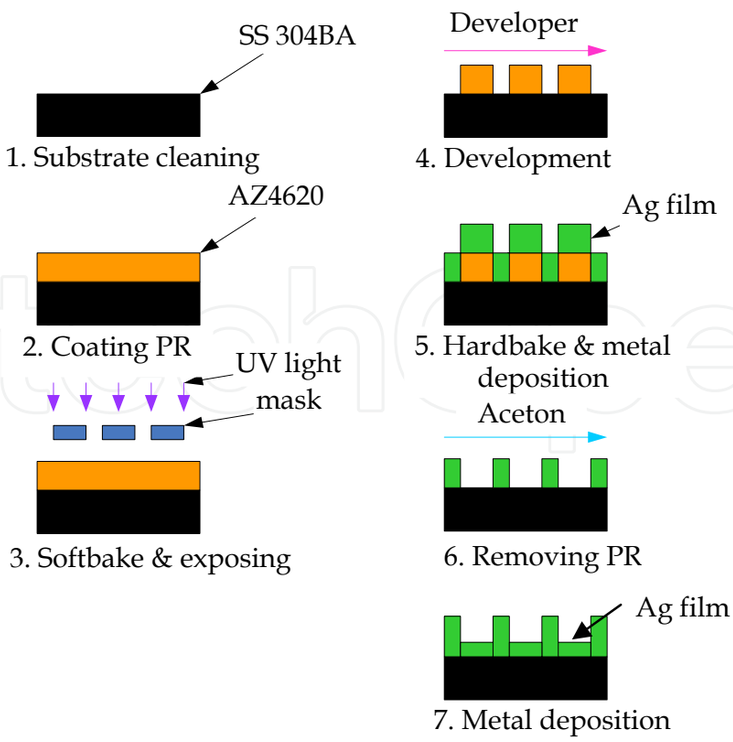

Fig. 4. The experimental flow charts of lift-off process.

Integrating Sphere is used for diffuse reflectance measurements. Reflectance measurements include total and diffuse reflectance at an incident angle of 8 degrees. Specular reflectance can be calculated from the total and diffuse reflectance measurements. The TR and DR rate of a textured substrate are important indexes when increasing the light trapping efficiency of thin-films solar cells.

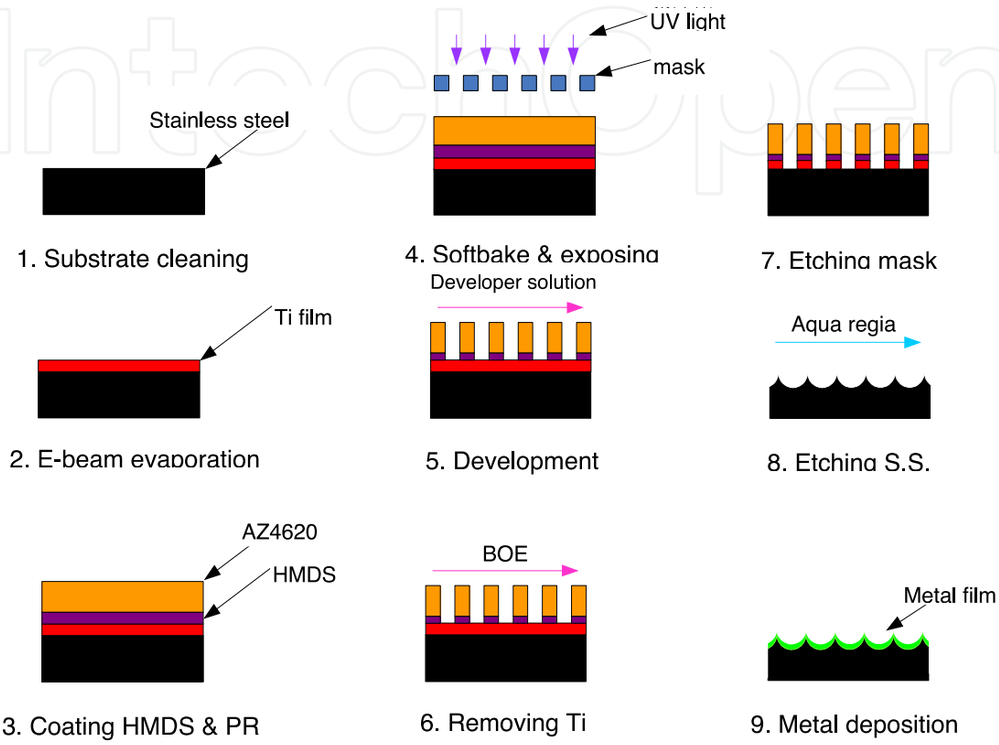

Fig. 5. The experimental flow charts of etching process.

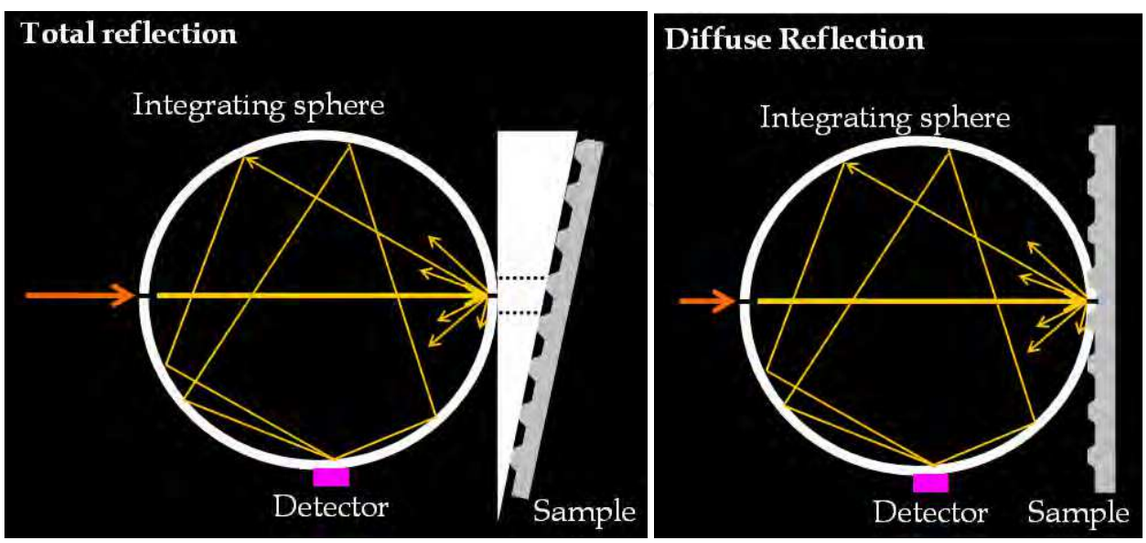

Fig. 6. The total reflection and diffuse reflection measured by integrating Sphere.

3.2 Optical properties on periodically textured 430BA stainless steel substrate

Lately the light trapping properties of textured substrates have attracted substantial interest because of their potential to reduce the thickness of solar cell material. In this study, the different kinds of textured patterns formed on 430BA SS substrate have been proposed for the purpose of trapping light in the application of thin film solar cells. Figure 7 shows the surface morphology of the 430BA SS substrate etched by using aqua regia. It should be noted that the dark and light regions of the OM images indicate the concave structure and the flat surface on the textured 430BA SS substrate, respectively.

In order to understand the optical reflection of a textured 430BA SS substrate, the Perkin Elmer Lambda 900 spectrometer was used to analyze both the TR and DR rates of incident light. The TR and DR rates versus the wavelength curves for the raw and textured 430BA SS substrates are shown in Fig. 8 and Fig. 9, respectively. The "D" and "G" indicate the diameter and the gap for these periodically textured 430BA SS substrates, respectively. It must be noted that the discontinued data line in the wavelength of 850 to 950nm was due to the change in detector, from a PMT to a PbS detector. First, we compared the textured 430BA SS substrates with different diameters of 2, 4 and 6μm and with the same interval of 3μm. In Fig. 8, it was found that the DR rate at the wavelength of 600nm increases substantially, from 4.5% of a raw 430BA SS substrate to 19.7 %, 23.1% and 31.8% for textured 430BA SS substrates with a diameter of 2, 4 and 6μm, respectively. It was evident that for the same areas of analysis, the larger the size of the concave shape, the worse the TR rate would

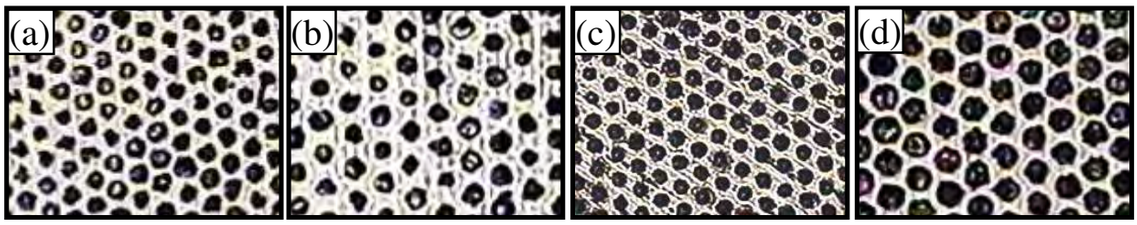

Fig. 7. The OM images of a concave periodically textured 430BA SS substrate with a diameter/gap of (a) 4/5 μm (b) 4/7 μm (c) 4/3 μm (d) 6/3 μm.

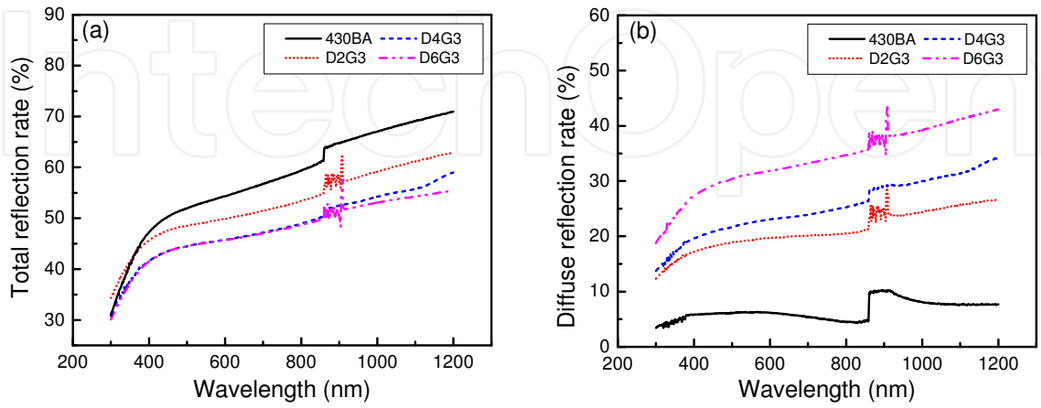

Fig. 8. The TR and DR rates versus the wavelength curves for raw 430BA SS substrate at different diameter of textured 430BA SS substrate.

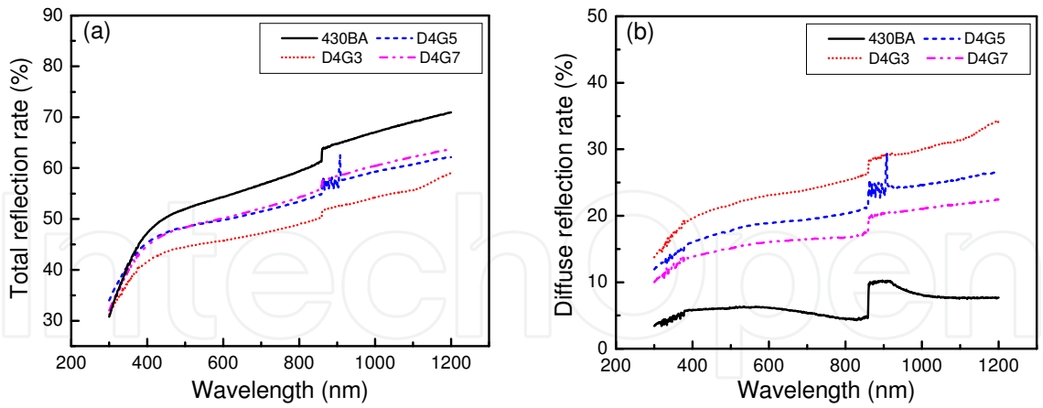

Fig. 9. The TR and DR rates versus the wavelength curves for raw 430BA SS substrate at different intervals of textured 430BA SS substrate.

be, resulting in a better diffuse reflection rate. We also investigated the TR and DR rates of the textured 430BA SS substrate with a different interval for samples with a fixed diameter of 4μm. In Fig. 9 we found that the DR rate at the wavelength of 600 nm decreased from 23.1% for a diameter/gap of 4/3 μm textured 430BA SS substrate to 18.9% and 16.1% respectively for a diameter/gap of 4/5μm and 4/7μm textured 430BA SS substrates. The decrease of the DR rate is related to the increase in the interval of the concave substrate.

The textured surface of the 430BA SS substrate leads to a lower TR rate compared to a specular surface of raw 430BA SS substrate. The lowering of the TR rate for the textured surface of the 430BA SS substrate can be understood on the basis of (a) the multiple scattering as a result of the multiple reflections from the textured surface of the 430BA SS substrate and a concomitant reduction in light intensity at each reflection due to the finite value of reflectance for 430BA SS, (b) light trapping in the indentations of a highly textured surface. Therefore, the results show that the textured 430BA SS substrate can generate a random distribution of light by reflection from a textured surface.

It is known that the incident light is reflected back into the cell for a second pass and subsequent passes. This phenomenon results in enhanced absorption in the cell. Thus, a back reflector should possess high reflectance in the solar part of the spectrum, which makes Ag a good candidate. Thus, we also performed the Ag coating on a textured 430BA SS substrate to study the TR and DR rates of incident light. The TR and DR rates versus the wavelength of textured 430BA SS with a silver film thickness of 300 nm are shown in Fig. 10. The peak at around 325 nm can be attributed to the diffuse reflectance spectrum of the deposited Ag film on the surface of the textured 430BA SS substrate (Xiong et al. 2003). In Fig. 10, the DR rate at the 600 nm wavelength are 40.6%, 47.2% and 64.6%, respectively for a diameter/gap of 2/3, 4/3 and 6/3 μm Ag film coated/textured 430BA SS substrate. The DR rate of Ag film coated/textured 430BA SS substrate increased about 2 times in comparison with the uncoated textured 430BA SS substrate (see Fig. 8). Similar results were also observed in Fig. 11 for the Ag film coated/textured 430BA SS substrate with a different interval for samples with a fixed diameter of 4μm. In addition, the TR rate increased to more than 90% for the Ag film coated/textured 430BA SS substrate which was an 80% improvement over the uncoated textured 430BA SS substrate.

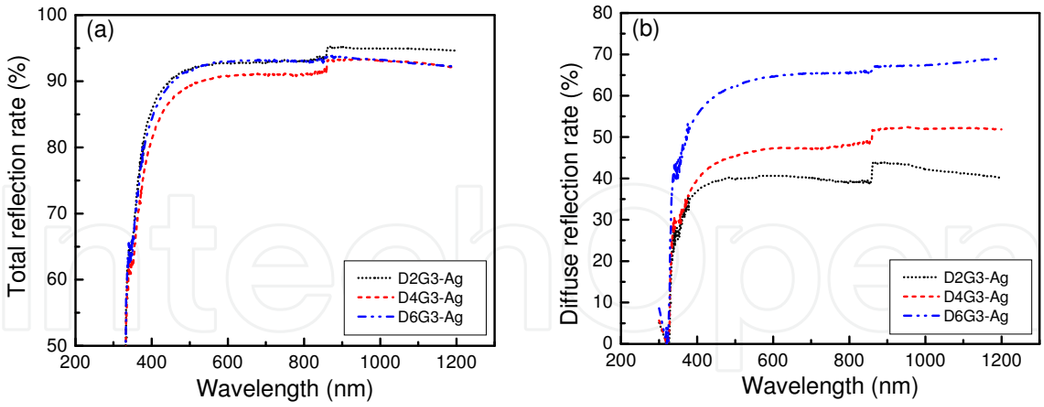

Fig. 10. The TR and DR rates versus wavelength curves for Ag film deposited at different diameter of textured 430BA SS substrate.

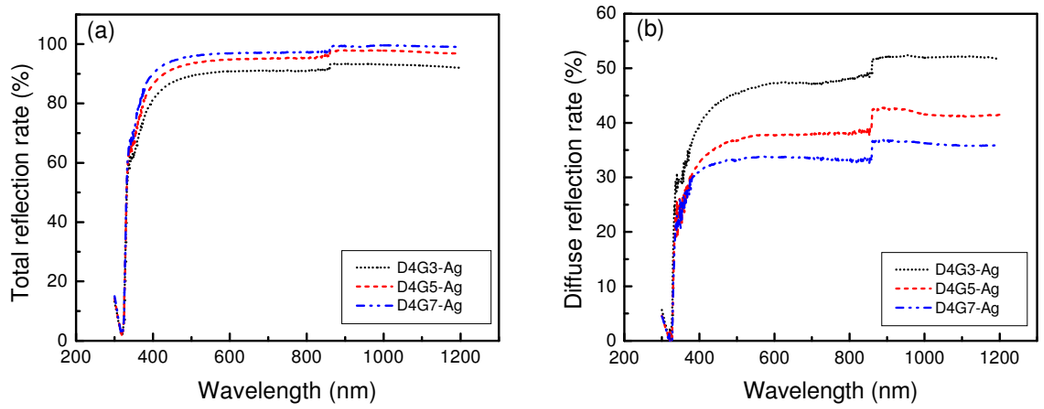

Fig. 11. The TR and DR rates versus wavelength curves for Ag film deposited at different intervals of textured 430BA SS substrate.

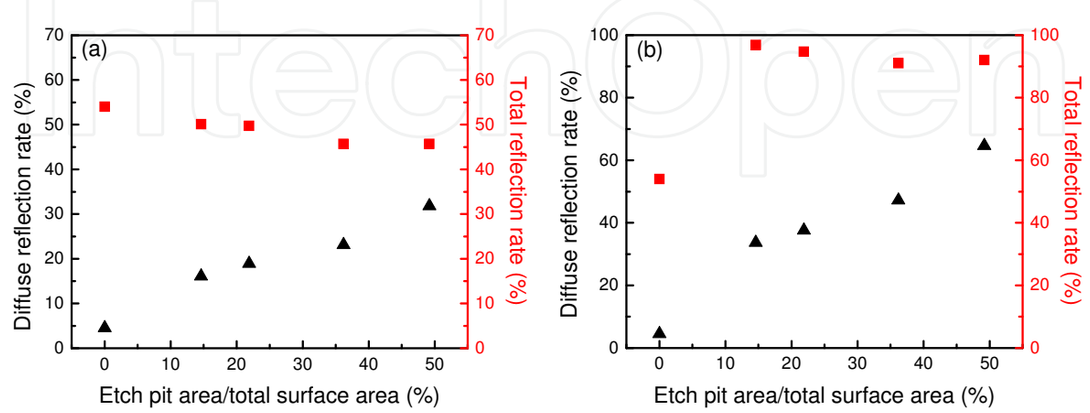

Fig. 12. The TR and DR rates as a function of the ratio of the etch pit area to the total surface area for (a) the textured 430BA SS and (b) the Ag film coated/textured 430BA SS.

From Fig. 8, it is evident that the TR and DR rates are not only dependent on the size of the concave shape but also depend on the interval of the concave substrate. Fig. 12(a) and (b) show the TR rate and DR rates as a function of the ratio of the etch pit area to the total surface area for the textured 430BA SS and the Ag film coated/textured 430BA SS, respectively. The ratio of the etch pit area to the total surface area is calculated by the number of pit in the total surface area multiplied by the single pit area divided by the total surface area. The total surface area is the analysis area in the spectrometer, measuring 1 cm^2. It is evident that the DR rate increased with the increase effectiveness of the pit regions compared to the smooth regions for both the textured 430BA SS and the Ag film coated/textured 430BA SS. However, the TR rate showed the opposite trend compared with the DR rate and decreased with the increase of the ratio of the etch pit area to total surface area. It is worth noting that once again the TR rate for the the Ag film coated/textured 430BA SS was more than 90% even the ratio of the etch pit area to the total surface area was 50%.

As shown in Figs. 8-11, we found that the increase in TR and DR rates as increase in light wavelength differed in the infrared range. The TR and DR rates clearly increased with the increasing light wavelength of the textured 430BA SS substrate. However, the TR and DR rates didn't increase with the increasing light wavelength of the Ag film coated/textured 430BA SS substrate. Huang et al. indicated that a metal with a lower work function can enhance the Raman signal of diamond films, which is referred to as surface-enhanced Raman scattering (SERS) (Huangbr et al. 2000). A very similar effect, surface-enhanced infrared absorption (SEIRA) was reported to occur with thin metal films (Hartstein et al. 1980, Hatta et al. 1982, Osawa 1997). Moreover, it was reported that the enhancement depends greatly on the morphology of the metal surface (Nishikawa et al. 1993). Fig. 13 shows the SEM image of an Ag film coated/textured 430BA SS substrate. It was found that the surface was covered with Ag particles ranging in size from tens to hundreds of nanometers. Thus, we believe that the difference in increase of the TR and DR rates in the infrared range for the textured 430BA SS and the Ag film coated/textured 430BA SS reflectors are due to the absorption in the infrared range by the Ag films. Further, the surface morphology was related to the thickness of the Ag film and must be carefully investigated in future study.

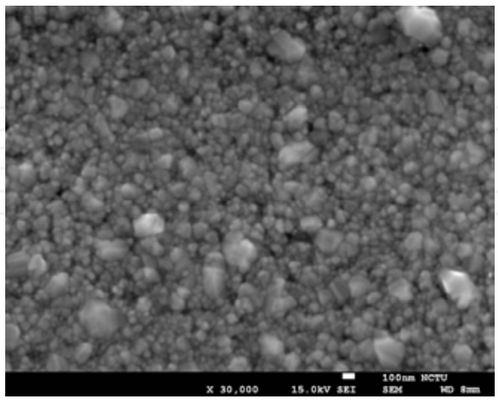

Fig. 13. The SEM image of Ag film coated/textured 430BA SS substrate.

3.3 Optical properties on periodically textured 304BA stainless steel substrate

Fig. 14 shows the OM images of the striped texture on the 304BA SS substrate. There are four patterns (i.e. the period/depth of 12/0.1, 12/0.3, 6/0.1, and 6/0.3 μm) which are designed and

used to study the TR and DR rates of the 304BA SS substrate. The stripe width and depth of the samples were measured by a surface profiler. The TR and DR rates versus the wavelength curves for untreated and the stripe-textured 304BA SS substrates are shown in Fig. 15. The "P" and "D" indicate the period and the depth for the periodically textured 304BA SS substrates, respectively. It was found that the DR rate at the wavelength of 600 nm increased substantially, from 3.5% of an untreated 304BA SS substrate to 10.5%, 21.8%, 18.2% and 39.4% for textured 304BA SS substrates with a period/depth of 12/0.1, 12/0.3, 6/0.1, and 6/0.3 μm, respectively. In addition, the TR rate of the untreated 304BA SS was 67.7% and increased to ~97% for the striped textured 304BA SS substrate due to the high reflection of the Ag film on its surface. It was evident that for the same areas of analysis, the smaller the period and the larger the depth, the better the DR rate would be, resulting in a better diffuse reflection rate.

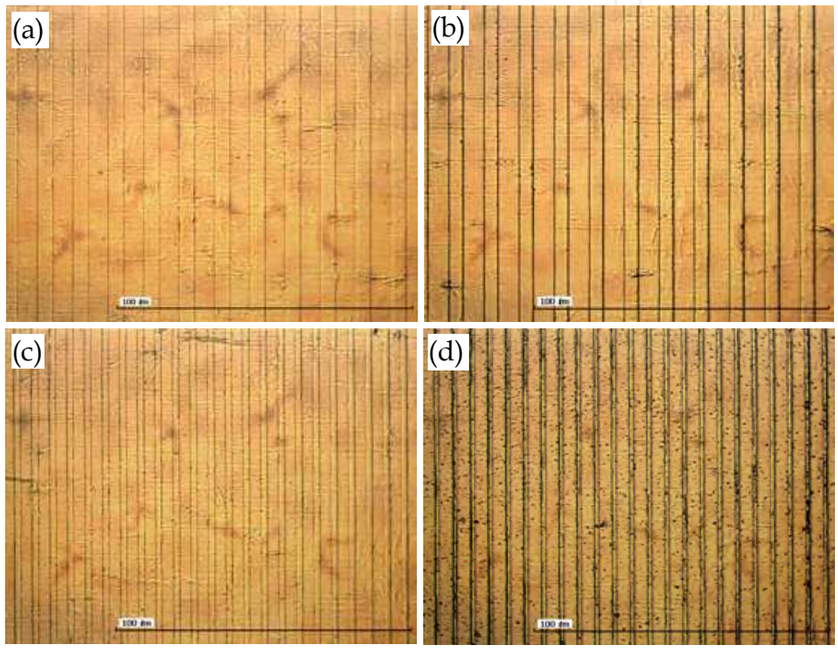

Fig. 14. The OM images of the stripe-textured 304BA SS substrate with a period/depth of (a) 12/0.1 μm (b) 12/0.3 μm (c) 6/0.1 μm (d) 6/0.3 μm.

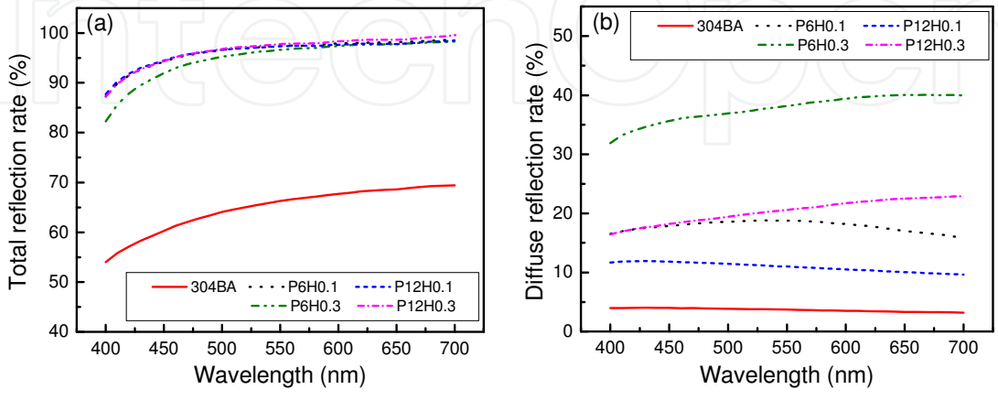

Fig. 15. The TR and DR rates versus the wavelength curves for untreated and stripe-textured 304BA SS substrates.

In our previous study (Lee et al. 2009), it was found that for a textured 430BA SS substrate the DR rate increased with the increased effectiveness of the etch-pit regions compared to that of the smooth regions. Thus, the large and deeply etched areas of the textured 304BA SS indicated that they can improve the DR rate of a textured 304BA SS substrate. In order to improve the DR rate even further, we design two other kinds of textured 304BA SS substrates, the ridged-stripe and the pyramid texture. 3D images of the ridged-stripe and pyramid texture are shown in Figs. 16(a) and (b), respectively. The etching depth and the width for both textured 304BA SS substrates were estimated to be ~6.5 μm and ~22.5 μm, respectively. The aspect ratio (i.e. depth/width) was ~1/3.5 indicating that the opening angle α of the textured surface was about ~120^{o}. It should be noted that the etching depth is controlled by the PR thickness and the etching time. In general, a thick PR and a long etching time can create the deeper textured 304BA SS substrate.

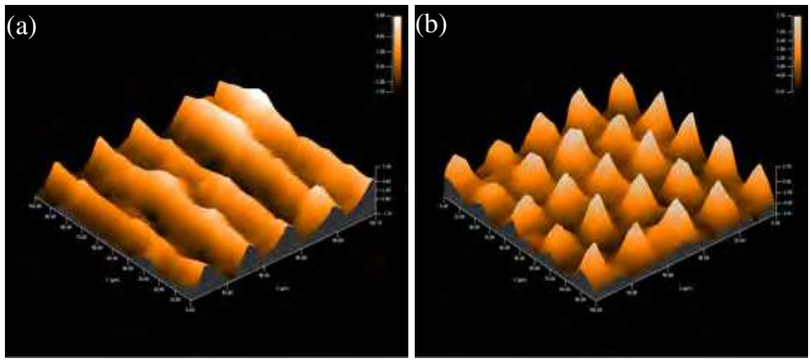

Fig. 16. The 3D images of (a) ridged-stripe and (b) pyramid 304BA SS substrate.

The TR and DR rates of the ridged-stripe and pyramid textured 304BA SS substrates are shown in Fig. 17. We found that the DR rate at the wavelength of 600 nm increased from 3.5 % for the untreated 304BA SS substrate to 60.1% for the pyramid and 63.1% for the ridged-stripe textured 304BA SS substrate. In addition, the DR rate also increased 1.5 times at the period/depth of 6/0.3 μm for the stripe-textured 304BA SS substrate. However, the textured substrates had a lower TR rate compared to the untreated 304BA SS substrate. The lowering of the TR rate for the textured surface of the 304BA SS substrate can be explained as follows (a) the multiple scattering is the result of the multiple reflections from the ridged-stripe or pyramid textured surface of the 304BA SS substrate, and the etching pit reduction in light intensity at each reflection is due to the finite value of the reflectance for the 304BA SS substrate, (b) light trapping occurs in the indentations of a highly textured surface. Therefore, the results show that the textured 304BA SS substrate can generate a random distribution of light through reflection from a textured surface.

It is well known that the incident light is reflected back into the cell for a second pass and subsequent passes. This phenomenon results in enhanced absorption in the cell. Thus, a back reflector must possess high reflectance in the solar part of the spectrum, making Ag or Al good candidates. However, Al films absorb the incident light wavelength of 800 nm and reduce the light conversion efficiency. On the other hand, the reflection of Ag film can achieve 99% from the visible to the IR wavelength (Jenkins and white 1957). Thus, we also used an Ag coating on a textured 304BA SS substrate to study the TR and DR rates of incident light. The TR and DR rates versus the wavelength of ridged-stripe and pyramid textured 304BA SS substrates with a silver film thickness of 150 nm are shown in Fig. 18. The

DR rates at the 600 nm wavelength were 95.6% and 96.8%, for the ridged-stripe and pyramid Ag film coated/texture 304BA SS substrates, respectively. The DR rate increased about 15-fold in comparison with the Ag coated untreated 304BA SS substrate. In addition, the TR rates at the 600 nm wavelength were 96.7% and 96.8%, for the ridged-stripe and pyramidal Ag film coated/texture 304BA SS substrates, respectively.

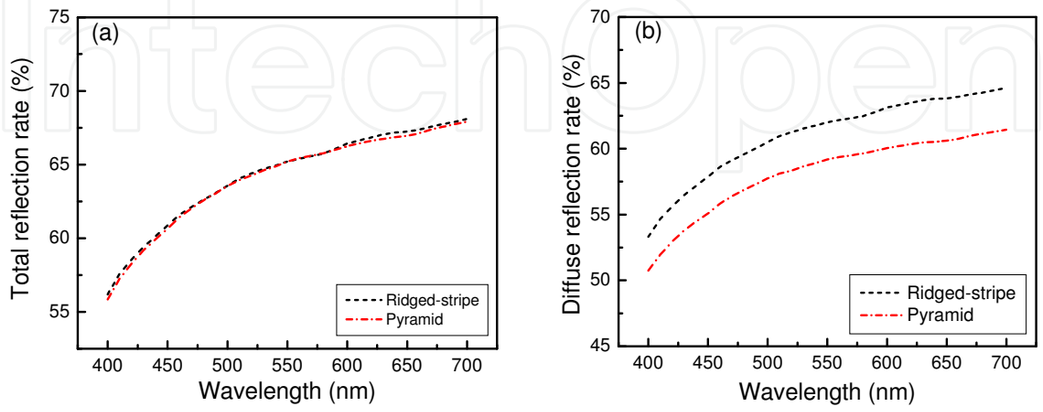

Fig. 17. The TR and DR rates versus the wavelength curves for ridged-stripe and pyramid textured 304BA SS substrates.

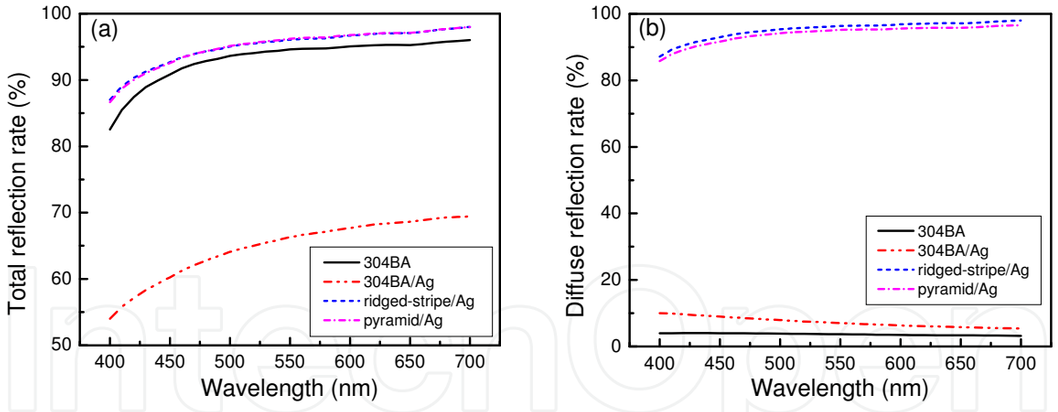

Fig. 18. The TR and DR rates versus the wavelength curves for Ag films coated/untreated 304BA SS substrate and Ag film coated/ridged-stripe and pyramid textured 304BA SS substrates.

Fig. 19 shows the relationship between the DR/TR rates and the total effective area of the Ag film coated/textured 304BA SS substrate. It should be noted that the total effective area was defined by the incident light reaching the textured 304BA SS substrate in an area of 100×100 μm². For example, the total effective area of the stripe textured 304BA SS substrate was calculated by the etched side wall area added to the untreated area of 10000 μm². For the ridged-stripe textured 304BA SS, the total effective area was calculated by summing the

nine ridged-surfaces within an area measuring 100×100 μm^2. For the pyramid textured 304BA SS substrate, the total effective area was calculated by adding 25 pyramid-textured surfaces to the no-pyramid-coverage areas. Since the high reflection property of Ag films, the TR rate was almost higher than 90% after Ag-film coating of the textured 304BA SS substrates. It is worth noting that the DR rate increased linearly with the increase in total effective area of the stripe-textured 304BA SS substrate. However, the increase of the DR rate with the increase in the total effective area for the ridged-stripe and pyramid textured 304BA SS substrate was much more dramatic. We believe that the dramatic increase in the DR rate was due to the fact that the textured surface generated a random distribution of light by reflection from the textured surface. The aspect ratio for the ridged-stripe and pyramidal textured 304BA SS substrate were about 1/3.5 with an opening angle of 120^o. In addition, the diffuse rate was defined when the incident light angle was zero, and the reflection light of that angle was larger than 8^0 over the incident light. Thus, the increased light diffuse due to the 120^o opening angle of the texture surface caused the dramatic increase of the DR rate for the ridged-stripe and pyramid textured 304BA SS substrate. In addition, weakly absorbed light is totally reflected internally at the top surface of the cell as long as the angle of incidence inside the a-Si at the a-Si/TCO interface is greater than 16^0 (Banerjee and Guha 1991). It was indicated that the tilt angle of the V-shaped light trapping configuration substantially increases the photocurrent generation efficiency (Rim et al. 2007). The photocurrent increased with the increase of the tilt angle of the V-shaped configuration and is believed to enhance the number of ray bounces per unit cell area over that in a planar structure at each point in the V-fold structure. Therefore, the tilted angle of the textured surface is related to the DR and TR rate, and must be carefully investigated in future study.

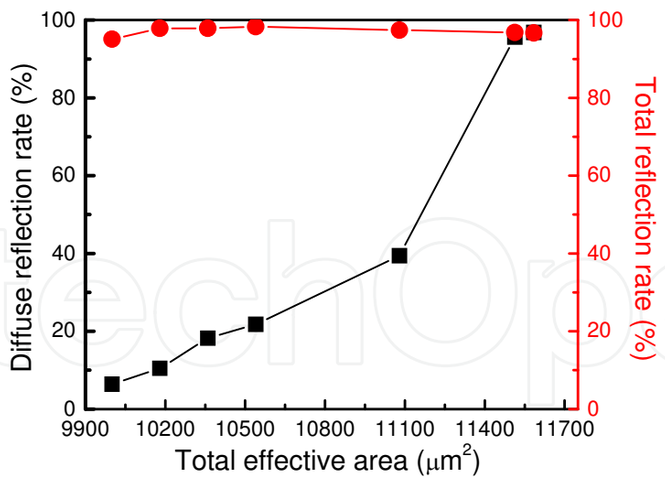

Fig. 19. The TR and DR rates as a function of the total effective area for Ag films coated on textured 304BA SS substrates.

4. Conclusions

We have demonstrated that a large diameter or a small interval of a concave shaped structure made from textured 430BA SS substrate can improve the DR rate of light.

However, the textured surface of a 430BA SS substrate led to a lower TR rate compared to a specular surface of raw 430BA SS substrate. This was due to the trapping of light in the hollows of the highly textured surface. Moreover, coating the textured 430BA SS substrate with an Ag film substantially improved not only the DR rate but also the TR rate of the incident light. The slow increase of the TR and DR rates versus the wavelength in the IR region of the Ag coated/textured 430BA SS substrates was due to the Ag absorption effect. We believe that Ag coated/textured 430BA SS substrates can generate a random distribution of light, increase the light trapping efficiency and be applied in thin films solar cells.
In addition, the DR and TR rate of the stripe, ridged-stripe and pyramid textured 304BA SS substrate were investigated to determine the optimal surface for increasing their light trapping efficiency. The DR rate increased with the increase in the total effective area of the Ag film coated/stripe textured 304BA SS substrate. It is believed that the tilt angle of the textured 304BA SS substrate increases the DR rate. The experimental results showed that the DR rate and the TR rate of the Ag film coated/ ridged-stripe textured 304BA SS substrate can achieve up to ~97% and 98% efficiency, respectively. The DR and TR rate of the Ag film coated/ridged-stripe textured 304BA SS substrates increased 28-fold and 1.4-fold, respectively, compared with the untreated 304BA SS substrate. The drastically increased DR rate is due to not only the increase in total effective area, but also to the decrease in the opening angle of the ridged textured substrate which generates a more random distribution of light by scattering.

5. Acknowledgment

The authors gratefully acknowledge the financial support from the National Science Council of Taiwan, R.O.C. under Contract No. NSC-98-2112-M155-001-MY3 and NSC-99-2221-E-155-065.

6. References

Banerjee A. and S. Guha. (1991). Study of back reflectors for amorphous silicon alloy solar cell application. *J. Appl. Phys.,* Vol. 69, pp. 1030., ISSN: 1089-7550

Curtin Benjamin, Rana Biswas, and Vikram Dalal. (2009). Photonic crystal based back reflectors for light management and enhanced absorption in amorphous silicon solar cells. *Appl. Phys. Lett.* Vol. 95, pp. 231102., ISSN: 1077-3118

Chau Joseph Lik Hang, Ruei-Tang Chen, Gan-Lin Hwang, Ping-Yuan Tsai and Chien-Chu Lin. (2010). Transparent solar cell window module. *Sol. Energy Mater. Sol. Cells.,* Vol. 94, pp. 588., ISSN: 0927-0248.

Deckman H. W., C. R. Wronski, H. Wittzke, and E. Yablonovitch. (1983). Optically enhanced amorphous silicon solar cells. *Appl. Phys. Lett.,* Vol. 42, pp. 968., ISSN: 1077-3118.

Ferlanto A. S., G. M. Ferreira, J. M. Pearce, C. R. Wronski, R. W. Collins, X. Deng, and G. Ganguly. (2002). Analytical model for the optical functions of amorphous semiconductors from the near-infrared to ultraviolet: Applications in thin film photovoltaics. *J. Appl. Phys.,* Vol. 92, pp. 2424., ISSN: 1089-7550

Fung Taddy Y. Y. and H. Yang. (2008). Study on thermal performance of semi-transparent building-integrated photovoltaic glazings. *Energy and Buildings.,* Vol. 40, pp. 341-350., ISSN: 0378-7788.

Hartstein A., J. R. Kirtley, J. C. Tsang. (1980). Enhancement of the Infrared Absorption from Molecular Monolayers with Thin Metal Overlayers. *Phys. Rev. Lett*., Vol. 45, pp. 201. , ISSN: 1079-7114

Hatta A., T. Ohshima, W. Suëtaka. (1982). Observation of the enhanced infrared absorption of p-nitrobenzoate on Ag island films with an ATR technique. *J. Appl. Phys. A*., Vol. 29, pp. 71., ISSN: 2158-3226

Huang B. R., K. H. Chen, W. Z. Ke. (2000). Surface-enhanced Raman analysis of diamond films using different metals. *Mater. Lett*., Vol.42, pp. 162., ISSN:0167-577X

He Chun, Ya Xiong, Jian Chen, Changhong, Xihai Zhu. (2003). Photoelectrochemical performance of Ag–TiO_2/ITO film and photoelectrocatalytic activity towards the oxidation of organic pollutants. *J. Photochem. Photobiol. A*., Vol. 57, pp. 71., ISSN: 1010-6030

Jenkins F. A. and H. E. White. (McGraw Hill, New York, 1957). *Fundamentals of Optics*., P. 522. ISBN: 0070-8534-60

John A. E. St., U. S. Patent No. 3 487 223

Llopis F. and I. Tobías. (2005). The role of rear surface in thin silicon solar cells. *Sol. Energy Mater. Sol. Cells.,* Vol. 87, pp. 481., ISSN: 0927-0248

Lee Shuo Jen, Shiow Long Chen, Cheng Wei Peng, Chih Yuan Lin, Wen Cheng Ke. (2009). Enhanced diffuse reflection of light into the air using silver coating on periodically textured 430BA stainless steel substrate. *Mater. Chem. Phys.,* Vol. 118, pp. 219-222., ISSN: 0254-0584

Müller J., B. Rech, J. Springer and M. Vanecek (2004). TCO and light trapping in silicon thin film solar cells. *Sol. Energy*. Vol. 77, pp. 917., ISSN: 0038-092X

Nishikawa Y., T. Nagasawa, K. Fujiwara, M. Osawa. (1993). Silver island films for surface-enhanced infrared absorption spectroscopy: effect of island morphology on the absorption enhancement. *Vib. Spectrosc*., Vol. 6, pp. 43., ISSN: 0924-2031

Otte K., L. Makhova, A. Braun, I. Konovalov. (2006). Flexible Cu(In,Ga)Se_2 thin-film solar cells for space application. *Thin Solid Films*., Vol. 511, pp. 613., ISSN: 0040-6090

Osawa M. (1997). Dynamic Processes in Electrochemical Reactions Studied by Surface-Enhanced Infrared Absorption Spectroscopy (SEIRAS). *Bull. Chem. Soc. Jpn*., Vol. 70, pp. 2861., ISSN: 0009-2673

Rech B., O. Kluth, T. Repmann, T. Roschek, J. Springer, J. Müller, F. Finger, H. Stiebig, and H. Wagner. (2002). New materials and deposition techniques for highly efficient silicon thin film solar cells. *Sol. Energy Mater. Sol. Cells.,* Vol. 74, pp. 439., ISSN: 0927-0248

Rim Seung-Bum, Shanbin Zhao, Shawn R. Scully, Michael D. McGehee and Peter Peumans. (2007). An effective light trapping configuration for thin-film solar cells. *Appl. Phys. Lett.* Vol. 91, pp. 243501. ISSN: 1077-3118

Selvan J. A. Anna., A. E. Delahoy, S. Guo and Y. M. Li. (2006). A new light trapping TCO for nc-Si:H solar cells. *Sol. Energy Mater. Sol. Cells*., Vol. 90, pp. 3371., ISSN: 0927-0248

Sőderstrőm T., F. –J. Haug, V. Terrazzoni-Daudrix, and C. Ballif, J. (2008). Optimization of amorphous silicon thin film solar cells for flexible photovoltaics. *J. Appl. Phys.*, Vol. 103, pp. 114509-1., ISSN: 1089-7550

Yablonovitch E. and G. Cody. (1982). Intensity enhancement in textured optical sheets for solar cells. *IEEE Trans. Electron. Devices ED.*, Vol. 29, pp. 300., ISSN: 0018-9383

Zhou Dayu and Rana Biswas. (2008). Photonic crystal enhanced light-trapping in thin film solar cells. *J. Appl. Phys.*, Vol. 103, pp. 093102. , ISSN: 1089-7550

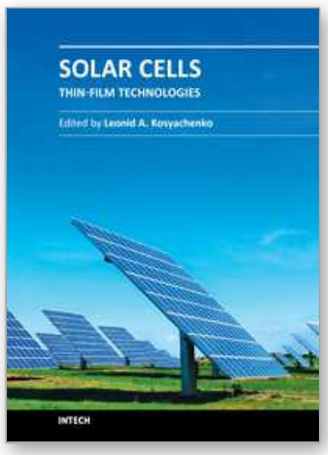

Solar Cells - Thin-Film Technologies

Edited by Prof. Leonid A. Kosyachenko

ISBN 978-953-307-570-9
Hard cover, 456 pages
Publisher InTech
Published online 02, November, 2011
Published in print edition November, 2011

The first book of this four-volume edition is dedicated to one of the most promising areas of photovoltaics, which has already reached a large-scale production of the second-generation thin-film solar modules and has resulted in building the powerful solar plants in several countries around the world. Thin-film technologies using direct-gap semiconductors such as CIGS and CdTe offer the lowest manufacturing costs and are becoming more prevalent in the industry allowing to improve manufacturability of the production at significantly larger scales than for wafer or ribbon Si modules. It is only a matter of time before thin films like CIGS and CdTe will replace wafer-based silicon solar cells as the dominant photovoltaic technology. Photoelectric efficiency of thin-film solar modules is still far from the theoretical limit. The scientific and technological problems of increasing this key parameter of the solar cell are discussed in several chapters of this volume.

INTECH
open science | open minds

InTech Europe
University Campus STeP Ri
Slavka Krautzeka 83/A
51000 Rijeka, Croatia
Phone: +385 (51) 770 447
Fax: +385 (51) 686 166
www.intechopen.com

InTech China
Unit 405, Office Block, Hotel Equatorial Shanghai
No.65, Yan An Road (West), Shanghai, 200040, China
中国上海市延安西路65号上海国际贵都大饭店办公楼405单元
Phone: +86-21-62489820
Fax: +86-21-62489821

IntechOpen